Development of a cold spot joining method that enables sound joining of carbon steel below the A_1 temperature

Takumi Aibara[a], Yoshiaki Morisada[a] and Hidetoshi Fujii[a]*

[a]*Joining and Welding Research Institute, Osaka University, 11-1 Mihogaoka, Ibaraki, Osaka 567-0047, Japan*

* fujii.hidetoshi.jwri@osaka-u.ac.jp

Development of a cold spot joining method that enables sound joining of carbon steel below the A_1 temperature

A novel solid-state joining method, which we call cold spot joining (CSJ), was successfully developed. In this joining concept, the material in the vicinity of the interface is plastically deformed using high pressure to form the joining interface, and impurities at the interface are expelled to the outside. Medium-carbon steel sheets were joined using the CSJ method under various process conditions. The joining temperature can be modified by the pressure applied during CSJ. Microstructural observations and hardness distributions revealed that proper pressurisation led to a joining temperature below the A_1 point and prevented the formation of brittle martensitic phase. A sound S45C joint showing plug rupture at the base metal under both tensile shear and cross-tension tests was successfully fabricated by providing appropriate applied pressure and energising conditions.

Keywords: solid-state joining; non-transformation joining; spot joining method; carbon steel, pressure control; microstructure; mechanical properties

1. Introduction

Improving safety and reducing environmental impact are essential goals in the automotive industry. Increasing the strength of automobile body materials is a very effective means of solving these issues, as it simultaneously improves collision safety and fuel economy by reducing the weight of the automobile body [1–4]. Because increasing the carbon content of steels and applying appropriate microstructural tailoring, including incorporation of microalloy additions in advanced automotive sheet steels, can provide good strength, carbon steels are considered promising structural materials for use in the automotive industry. However, for medium- and high-carbon steels, obtaining sound weld joints by fusion welding is difficult owing to the formation of the brittle martensitic phase upon cooling from a high temperature (above the phase transformation point, A_1), which may cause cracking in the weld zone [5]. Therefore, solid-state joining techniques with a low welding temperature below the A_1 point are

required to join medium- and high-carbon steels [6,7].

The predominant methods utilised in the automotive industry to produce car body are spot joining methods such as resistance spot welding (RSW) [8,9]. RSW is a fusion welding method in which a metal sheet is clamped between copper electrodes, and a large current is applied for a short time to form a molten area between the metal sheets to achieve bonding. Research has indicated the potential of post-heating tempering to enhance the strength of joints [10–12]. However, this technique presents certain challenges. Notably, the limited range of permissible tempering temperatures necessitates precise control [13]. Furthermore, this method often leads to extended joining durations, posing a potential hurdle to efficient production. Spot joining methods that achieve joining in the solid state include mechanical joining processes, such as self-piercing rivets and mechanical clinching [14,15], and solid-state welding technologies, such as friction element welds and friction stir welding [9,16]. Nevertheless, there have been few successful attempts to spot join medium- or high-carbon steel sheets with a carbon content exceeding 0.3% using these solid-state joining techniques to achieve high-strength joining.

In light of these issues, we propose a novel joining concept in which the material near the interface is plastically deformed using high pressure to form the joining interface, and impurities at the interface are ejected to the outside. Moreover, because a higher pressure is applied, the interface materials can be deformed at lower temperatures, thereby allowing the joining temperature to be lower than the A_1 point. This concept has been verified in our previous studies on linear friction welding (LFW) [17], rotary friction welding (RFW) [18], and pressure-controlled joule-heat forge welding (PJFW) [19].

In this study, a novel joining apparatus was designed for the proposed process, which we call cold spot joining (CSJ). Medium-carbon steel sheets were joined using the CSJ method, and the effects of the process parameters on the microstructure and mechanical properties of the joints were systematically investigated to obtain a sound carbon steel joint at a low temperature, specifically, below the A_1 point.

2. Experimental procedures

Figure 1(a) shows the CSJ apparatus, which is composed of a DC inverter power supply (Amada Weld Tech IS-1400A), an inverter transformer (Dengensha MIR115-39060), an electric servo press (Coretec FMS100-B), a control panel, and a joining unit; the final two components were custom-made and are magnified in the red dotted rectangle. The maximum current of the power supply was 14,000 A at a maximum voltage of 10 V. The electric servo press provided a maximum load of 100 kN. A cross-sectional view of the CSJ joining apparatus is shown in Figure 1(b). The joining tools consist of two parts: a central pressure rod made of tungsten carbide, which is responsible only for applying pressure, and a cylindrical electrode made of a copper-chromium alloy, which is responsible only for energising the electrode. This dual structure allows for both energisation and the separate application of a large load. The centre pressure rod was pressurised using an electric servo press. The cylindrical copper electrode was pressurised using an air cylinder that was controlled separately from the central pressure rod. A cross-sectional view of the tip of the central pressure rod is shown in Figure 1(c). The tip of the central pressure rod has a tapered shape. A flat area with a diameter of 8 mm was extended 1 mm from the tip to ensure even pressure at the periphery. The copper electrode was cylindrical, with an outside diameter of 12 mm and an inner diameter of 10 mm. Sheets of medium-carbon steel, S45C (0.45 wt% C, 0.74 wt% Mn, 0.22 wt% Si, 0.12 wt% Cr, balance Fe), 1.6 mm thick were used as the base material

(BM). The surfaces of the specimens were acid-washed to remove the oxide film, polished using a No. 400 hand grinder, and degreased with acetone.

As a preliminary step before starting the joining of CSJ, a projection is formed at the centre of the joining area of the steel sheet using a central pressure rod. The protrusion is formed using a pressure rod of the same shape and a cylindrical mould with an inner diameter of 6 mm, which is pressed 1 mm into the steel. This concentrates the electric current in the centre to facilitate deformation.

The steps of the joining process in CSJ are illustrated in Figure 1(d). First, while pressurising the steel sheet with the central pressure rod, the material is heated by passing an electric current through the copper electrode. As the temperature increases, the steel sheets soften, and deformation occurs when the strength at the interface decreases below the applied pressure. Second, the impurity layer on the surface of the steel sheet is expelled by the deformation, and a joining interface is formed. Finally, when the designated energising time or pressing amount is achieved, the pressure is released and the current is terminated to accomplish the joining process.

The pressure determined from the area of the joining interface and the pressure load was controlled to be constant by increasing the load on the central pressure rod in steps. The area of the joining interface was measured with a high-speed camera. Two methods were used for energising: constant current and constant power. The applied pressure was varied from 200 to 400 MPa, and the current was 2500 A. The energisation time was 35 s. In constant-power experiments, the power was controlled at 1500 W with applied pressures of 300 and 400 MPa. The pushing amount was set to 1.3 mm.

Longitudinal cross-sectional specimens were prepared from the fabricated joints. The specimens were mechanically polished using waterproof SiC emery papers of up to

4000 grit, followed by an electropolishing solution consisting of 10 vol% perchloric acid and 90 vol% acetic acid at 20 V for ~20 s. The electro-polished specimens were then observed using a scanning electron microscope (SEM; JEOL JSM-7001 FA) to characterise the joining interface microstructure. The Vickers hardness distributions along the joining interface and the two longitudinal axes on the cross-sectional specimens, as indicated by the red dotted lines in Figure 2(b), were measured with a load of 2.94 N for a dwell time of 15 s using a hardness tester (Future-Tech FM-800). Tensile tests were performed according to the JIS Z 3136 and JIS Z 3137 standards [20,21]. The geometries of the tensile test specimens for the tensile shear and cross-tension tests are shown in Figure 2(c,d). Tensile tests were performed at room temperature using a mechanical testing machine (Shimadzu Autograph AG-10 TB) at a cross-head speed of 10 mm/min. For each joining condition, three tensile samples were tested.

3. Results and discussion

3.1. Effect of applied pressure on the joint

3.1.1. Macrostructure and microstructure of the joining interface

Figure 3(a–c) shows macrographs of the cross-sections of the joints fabricated at different applied pressures of 200, 300, and 400 MPa with a constant 2500 A current and current-carrying time of 35 s. The heat affected zone (HAZ) is indicated by a yellow dotted line. In RSW, it is known that when welding is performed with a DC power source, the amount of heat generated on the positive side increases owing to the Peltier effect between the electrode and joined material [22]. Consequently, the upper HAZ region, which is toward the positive electrode, is wider. Figure 3(d–i) show the microstructure of the area indicated by the red squares in Figure 3(a–c). The

microstructure of the base material is shown in Figure 3(j). The centre and periphery at 200 MPa (Figure 3(d,e)) and the periphery at 300 MPa (Figure 3(g)) consisted mostly of martensitic microstructure. These results indicate that the joining temperature exceeded the A_1 point at the entire interface at 200 MPa and at the periphery at 300 MPa. The centre at 300 MPa (Figure 3(f)) and the centre and periphery at 400 MPa (Figure 3(h) and (i)) show a microstructure composed of refined ferrite grains and pearlite containing refined ferrite grains and rod- and particle-shaped cementite with no martensite, which suggests that dynamic recrystallisation occurred around the joining interfaces.

This microstructural observation is explained by the temperature dependence of the tensile strength of S45C, as shown in Figure 4 [17]. The tensile strength of S45C decreases with increasing temperature, decreasing to ~300 MPa when the temperature rises to ~680 °C. Based on these relationships, it is expected that if a pressure of 300 MPa is applied to the S45C sheets during the CSJ process, the joining zone is plasticised to form the joint when the temperature increases to ~680 °C, which allows the peak joining temperature to not exceed 700 °C, that is, remain below the A_1 point. However, as mentioned above, at 300 MPa, it was confirmed that although the joining temperature was below the A_1 point in the centre, it exceeded the A_1 point at the periphery. This can be explained as follows. Unlike spot welding, in the CSJ method, the copper electrode is placed at the periphery rather than the centre, resulting in uneven heat generation at the interface. Therefore, the heat generation rate was faster at the periphery than at the centre. According to the joining principle of the CSJ, the pressure rod pressurises the joining material and plastically deforms the joining interface to expel the impurity layer. When the joining material pressurised by the pressure rod reaches a deformable strength in the lowest-temperature region (the centre) of the joining interface, the joining material is deformed throughout the entire interface. Therefore, the

joining temperature increased at the periphery because appropriate pressure was not applied there. At 200 MPa, the deformation temperature of S45C is approximately 750 °C, as shown in Figure 4. Therefore, at 200 MPa, it can be presumed that the joining temperature was approximately 750 °C at the centre and higher at the periphery. Microstructural observations confirmed that martensitic structure was formed both in the centre and at the periphery, confirming that the joining temperature had exceeded the A_1 point. At 400 MPa, the deformation temperature of S45C is approximately 625 °C, which is lower than that at 300 MPa, and joining was achieved below the A_1 point at both the periphery and centre. Accordingly, it was concluded that the joining temperature could be successfully modified by selecting the applied pressure based on the temperature dependence of the material strength. A low joining temperature below the A_1 point was successfully achieved under the condition of 400 MPa.

3.1.2. Hardness distribution

Figure 5(a–c) shows the hardness distribution on the cross-sections of the joints fabricated at different pressures of 200, 300, and 400 MPa with a constant current of 2500 A. The hardness of the joining interface formed at 200 MPa increased over a wide region compared with that of the base metal. The hardness of the joining interface formed at 300 MPa was higher than that of the BM at the periphery, and the joining interface at the centre had a hardness comparable to that of the BM. The hardening area decreased with increasing applied pressure, and the entire joining interface formed at 400 MPa showed almost the same hardness as the BM. The area with high hardness matches the HAZ, which is indicated by the yellow dotted line in Figure 3. The microstructural observation in Figure 3 shows that a martensitic structure was formed in the HAZ, which can be considered to have increased the hardness. At 400 MPa, martensitic transformation was successfully suppressed throughout the interface, and a

homogeneous hardness distribution was obtained. In RSW of ultra-high-strength steel sheets with a high-carbon equivalent, it is known that hardness decreases at the molten boundary owing to the partitioning of solute atoms, such as carbon, from the solid fusion boundary to the molten weld nugget [23–25]. This hardness reduction is considered to decrease the cross-tension strength (CTS). However, a joint without a decrease in the material hardness was successfully obtained using CSJ.

3.1.3. Tensile property

Figure 5(d) shows the tensile shear strength (TSS) of the joints fabricated at 200, 300, and 400 MPa with a constant current of 2500 A. The TSS of the joint fabricated at 400 MPa resulted in the highest value, followed by 200 and 300 MPa. The joints fabricated under all the conditions fractured at the interface. To further understand the TSS results, the pressing amount of the pressure rod, joining interface diameter, and joining region diameter were investigated for each applied pressure condition. The pressing amount, joining interface diameter, and joining region diameter after joining at different applied pressures of 200, 300, and 400 MPa with a constant current of 2500 A are shown in Figure 3(k). Higher pressure led to a smaller pressing amount and a smaller joint interface diameter. The reason for the decrease in the pressing amount despite the higher applied pressure is that a higher applied pressure decreases the joining temperature. In contrast, the joining region diameter increased in the order of 300, 200, and 400 MPa. The reasons for this are as follows. Figure 3 shows that martensitic transformation occurred at the periphery at 200 and 300 MPa. It is known that crack propagation occurs easily in the martensitic microstructure of high-carbon-content steels, and crack propagation is expected to be easier in the joints formed at 200 and 300 MPa [26]. Therefore, at 200 and 300 MPa, cracks propagated along the joining interface at the periphery after joining, which was considered to have reduced the joining region

diameter. At 400 MPa, no martensitic microstructure was formed at the periphery, which suppressed crack propagation and resulted in the largest joining region diameter. Because TSS increases with increasing diameter of the joining area [8,27], it increased in the order of 300, 200, and 400 MPa. However, fracture occurred at the interface even for the joint fabricated at 400 MPa. It is known that defects and non-adhered regions are retained at the joining interfaces formed at an applied pressure of 400 MPa because the faying surface deformation is not sufficient to rupture and disperse the oxide layers sufficiently. These defects cause stress concentrations and rapid fracture along the joining interface during tensile loading. It is thus inferred that the joining interface deformation plays a critical role in the oxide layer fragment and dispersion, fresh-metal-surface formation, adhesion and atomic bonding, and joining interface defect elimination during the CSJ process.

3.2. Effect of energising method on the joint

3.2.1. Macrostructure and microstructure of the joining interface

Figure 6 shows the joining interface microstructures of the joints fabricated at different applied pressures of 300 and 400 MPa with a constant power of 1500 W and constant pushing amount of 1.3 mm. Maintaining a constant power enables the current to increase as the resistance decreases, thereby reducing the decrease in temperature during the joining process and allowing the deformation to progress to the desired amount of pressing. The initial current was 2500 A at the start of the joining and increased to 3000 A at the end of the process. The diameter of the bonding interface was 8.8 mm at 300 MPa and 8.3 mm at 400 MPa, which is 1.3 times larger at both applied pressures based on a constant current of 2500 A. Constant power control enables the pressing amount to be increased by increasing the current during the joining process.

The periphery at 300 MPa (Figure 6(d)) exhibits mostly of martensite microstructure, whereas the centre at 300 MPa (Figure 6(c)) and the entire sample at 400 MPa (Figure 6(e,f)) show a microstructure composed of refined ferrite grains and pearlite-containing refined ferrite grains and rod- and particle-shaped cementite. This trend is consistent with the constant-current control, indicating that the applied pressure uniquely controls the joining temperature. A defect-free joint was successfully obtained under all pressure conditions. For both pressure conditions, the joining interfaces were further deformed to produce more fresh metal surfaces with further fragments, disperse the oxide layers, and enhance the adhesiveness between the joining interfaces, thereby promoting atomic bonding and eliminating the defects at the joint interface.

3.2.2. Hardness distribution

Figure 7(a–c) shows the hardness distributions on the cross-sections of the joints fabricated at different pressure conditions of 300 and 400 MPa with a constant power of 1500 W. The HAZ with a high hardness is indicated by the yellow dotted line in Figure 6. The hardness of the joining interface in the periphery fabricated at 300 MPa was higher than that of the BM, and the joining interface in the centre exhibited a hardness comparable to that of the BM. On the other hand, the joining interface fabricated at 400 MPa showed almost the same hardness as the BM at the entire interface. This result is consistent with the results for the constant-current control condition. Additionally, these results show that the joining temperature is controlled by the applied pressure, regardless of the energising conditions.

3.2.3. Tensile property

Figure 7(d) shows the TSS and CTS of the joints fabricated at 300 and 400 MPa with a constant power of 1500 W. The TSS of the joint was the highest at 400 MPa, reaching

14.9 kN and achieving a plug rupture. At 300 MPa, the TSS was 11.5 kN with interface rupture. Under both pressure conditions, the joining interface diameter increased compared to that of the constant current of 2500 A, successfully removing defects at the interface and improving the TSS. A similar trend was observed for the CTS, with plug rupture achieved at 6.8 kN at 400 MPa. At 300 MPa, the CTS was 2.1 kN, and interface fracture occurred. Figure 8 shows the results of the cross-sectional observations after the cross-tension test. The joint fabricated at 300 MPa exhibited crack propagation and rupture at the interface, whereas the joint fabricated at 400 MPa ruptured at the BM portion.

Interface rupture occurred despite the sufficient deformation of the interface at 300 MPa. The brittle martensitic structure formed at the periphery facilitates crack propagation at the interface. In contrast, plug rupture was achieved at 400 MPa by suppressing the formation of a brittle martensitic microstructure and by complete elimination of defects at the joining interface. According to JIS Z 3140 [28], which includes strength evaluation criteria, CTS should be 5.56 kN or more for mild steel, low-alloy steel, and high-tensile steel with a sheet thickness of 1.6 mm. In this study, a CTS higher than that of JIS Z 3140 was successfully obtained for medium-carbon steel, which is considered difficult to weld.

4. Conclusions

A CSJ method with plastic deformation of the joining interface was developed in this study. Strong interface bonding of the joint was possible below the A_1 point. This technique was carried out on 1.6 mm thick S45C medium-carbon steel at applied pressures of 200, 300, and 400 MPa with a constant current of 2500 A and power of 1500 W, and the following conclusions can be drawn.

(1) The joining temperature was successfully determined using applied pressure. At 400 MPa, strong joints were successfully formed below the A_1 point, and achieved a constant hardness of the joining interface.

(2) Maintaining constant power reduced the decrease in temperature during the joining process and allowed control of the deformation to the desired amount of pressing.

(3) Suppressing the formation of a martensitic microstructure at 400 MPa with 1500 W power and eliminating defects at the interface inhibited crack propagation to the interface and succeeded in obtaining a plug-ruptured joint in both shear and cross-tensile tests.

(4) This new CSJ method was successfully applied to joining S45C medium-carbon steel without any loss of material properties. It is expected that this joining method will enable high-strength joining not only of this material but also of all types of steels without compromising their material properties.

Acknowledgements

This work was supported by the JST-Mirai Programme under Grant number JPMJMI19E5; a Grant-in-Aid for Science Research from the Japan Society for the Promotion of Science under Grant number 19H00826; and the JST program for the establishment of university fellowships towards the creation of science technology innovation under Grant number JPMJFS2125.

Disclosure statement

The authors report there are no competing interests to declare.

Figure 1. (a) Cold spot joining (CSJ) apparatus. (b) Cross-sectional view of the CSJ unit apparatus. (c) Tip of the central pressure rod. (d) Schematic illustration of the joining process for CSJ. Step 1: Pressure is applied with the central pressure rod and the copper electrode. Step 2: Current is applied and the temperature rises at the interface. Step 3: The material temperature rises, and the pressure applied by the pressure rod deforms the bonding material. Step 4: When the desired pressing amount is reached, energising and pressurising are stopped and the bonding is completed.

Figure 2. Schematic illustration of specimen preparation for (a) Vickers hardness measurements, (b) tensile shear test, and (c) cross-tension test.

Figure 3. (a–c) Macrographs of cross-sections and scanning electron micrographs of the (d, f, h) joining interface centre and (e, g, i) periphery of the joints fabricated at applied pressures of 200, 300, and 400 MPa, respectively, with a constant 2500 A current. (j) Scanning electron microscopy image of the microstructure of S45C base material. (k) Pushing amount, joining interface diameter, and joining region diameter after joining at the applied pressures of 200, 300, and 400 MPa with a constant current of 2500 A.

Figure 4. Temperature dependence of ultimate tensile strength (UTS) of S45C [17].

Figure 5. Hardness distributions along the (a) joining interface, (b) longitudinal axis at the centre, and (c) longitudinal axis at 3.5 mm from the centre on cross-sections of the joints fabricated at applied pressures of 200, 300, and 400 MPa with a constant 2500 A current. (d) Tensile shear strength of the joints fabricated at applied pressures of 200, 300, and 400 MPa with a constant 2500 A current.

Figure 6. (a, b) Macrographs of cross-sections and (c–f) scanning electron micrographs of the joining interface centre and periphery of the joints fabricated at applied pressures of 300 and 400 MPa with a constant 1500 W power.

Figure 7. Hardness distributions along the (a) joining interface, (b) longitudinal axis at the centre, and (c) longitudinal axis at 3.5 mm from the centre on longitudinal cross-sections of the joints fabricated at different applied pressure of 300 and 400 MPa with constant 1500 W power. (d) Tensile shear strength (TSS) and cross-tension strength (CTS) of joints fabricated at different applied pressure of 300 and 400 MPa with constant 1500 W power.

Figure 8. Macrographs of cross-sections after the cross-tension test of the joints fabricated at different applied pressure of (a) 300 and (b) 400 MPa with constant 1500 W power. The yellow dotted line indicates areas of martensite.

References

[1] Matlock DK, Speer JG. Third generation of AHSS: microstructure design concepts. In: Haldar A, Suwas S, Bhattacharjee D, editors. Microstructure and texture in steels and other materials. Dordrecht, Netherlands: Springer; 2009. p. 185–205.

[2] Grajcar A, Kuziak R, Zalecki W. Third generation of AHSS with increased fraction of retained austenite for the automotive industry. Arch Civil Mech Eng. 2012;12(3):334–341.

[3] Pouranvari M, Marashi SPH. Critical review of automotive steels spot welding: Process, structure and properties. Sci Technol Weld Join. 2013;18(5):361–403.

[4] Shojaee M, Midawi ARH, Barber B, et al. Mechanical properties and failure behavior of resistance spot welded third-generation advanced high strength steels. J Manuf Process. 2021;65:364–372.

[5] Lippold JC. Welding metallurgy and weldability. New York (NY): Wiley; 2014.

[6] Fujii H, Cui L, Tsuji N, et al. Friction stir welding of carbon steels. Mater Sci Eng A. 2006;429(1–2):50–57.

[7] Cui L, Fujii H, Tsuji N, et al. Friction stir welding of a high carbon steel. Scripta Mater. 2007;56(7):637–640.

[8] Oikawa H, Murayama G, Hiwatashi S, et al. Resistance spot weldability of high strength steel sheets for automobiles and the quality assurance of joints. Weld World. 2007;51(3–4):7–18.

[9] Cai W, Daehn G, Vivek A, et al. A state-of-the-art review on solid-state metal joining. J Manuf Sci Eng. 2019;141(3):031012.

[10] Wei ST, Lv D, Liu RD, et al. Similar and dissimilar resistance spot welding of advanced high strength steels: welding and heat treatment procedures, structure and mechanical properties. Sci Technol Weld Join. 2014;19(5):427–435.

[11] Liu XD, Xu YB, Misra RDK, et al. Mechanical properties in double pulse resistance spot welding of Q&P 980 steel. J Mater Process Technol. 2019;263:186–197.

[12] Lv D, Xu X, Wang X, et al. Effect of tempering process on microstructure and properties of resistance spot-welded joints of δ-TRIP steel. Metals. 2022;12(12):2128.

[13] Taniguchi T, Furusako S, Kodama S. Examination of post-heating conditions to improve CTS in resistance spot-weld joints. Weld World. 2023;67:1359–1366.

[14] Li D, Chrysanthou A, Patel I, et al. Self-piercing riveting-a review. Int J Adv Manuf Technol. 2017;92:1777–1824.

[15] Abe Y, Kato T, Mori K, et al. Mechanical clinching of ultra-high strength steel sheets and strength of joints. J Mater Process Technol. 2014;214(10), 2112–2118.

[16] Matsui S, Ushioda K, Fujii H. Relationship between cross tension strength and carbon content of lower sheet in friction element welded steel joints. Weld Int. 2022;36(8):500–509.

[17] Kuroiwa R, Liu H, Aoki Y, et al. Microstructure control of medium carbon steel joints by low-temperature linear friction welding. Sci Technol Weld Join. 2020;25(1):1–9.

[18] Liu H, Aoki Y, Aoki Y, et al. Principle for obtaining high joint quality in dissimilar friction welding of Ti-6Al-4V alloy and SUS316L stainless steel. J Mater Sci Technol. 2020;46:211–224.

[19] Liu H, Miyagaki T, Lim Y, et al. A novel pressure-controlled joule-heat forge welding method to fabricate sound carbon steel joints below the A_1 point. J Manuf Process. 2021;68:770–777.

[20] Japanese Standards Association (JSA). Specimen dimensions and procedure for shear testing resistance spot and embossed projection welded joints. Tokyo: JSA; 1999. Standard No. JIS Z 3136:1999.

[21] Japanese Standards Association (JSA). Specimen dimensions and procedure for cross tension testing resistance spot and embossed projection welded joints. Tokyo: JSA; 1999. Standard No. JIS Z 3137:1999.

[22] Deng L, Li Y, Cai W, et al. Simulating thermoelectric effect and its impact on asymmetric weld nugget growth in aluminum resistance spot welding. J Manuf Sci Eng. 2020;142(9):091001.

[23] Ramachandran DC, Figueredo B, Sherepenko O, et al. A study on improving the mechanical performance by controlling the halo ring in the Q&P 980 steel resistance spot welds. J Manuf Process. 2022;75:320–330.

[24] Sherepenko O, Jüttner S. Transient softening at the fusion boundary in resistance spot welded ultra-high strengths steel 22MnB5 and its impact on fracture processes. Weld World. 2019;63(1):151–159.

[25] Sherepenko O, Kazemi O, Rosemann, P, et al. Transient softening at the fusion boundary of resistance spot welds: a phase field simulation and experimental investigations for Al–Si-coated 22MnB5. Metals. 2020;10(1):10.

[26] Yurioka N. Physical metallurgy of steel weldability. ISIJ Int. 2001;41(6):566–570.

[27] Ghassemi-Armaki H, Bhat S, Kelley S, et al. Quasi-static spot weld strength of advanced high-strength sheet steels: this study highlights the spot weld strength in tension-shear and cross-tension loading modes, and HAZ strength as a function of base metal strength, in sheet steels. Weld J. 2017;96(3):104s–112s.

[28] Japanese Standards Association (JSA). Method of inspection and acceptance levels for resistance spot welds. Tokyo: JSA; 1999. Standard No. JIS Z 3140:2017.

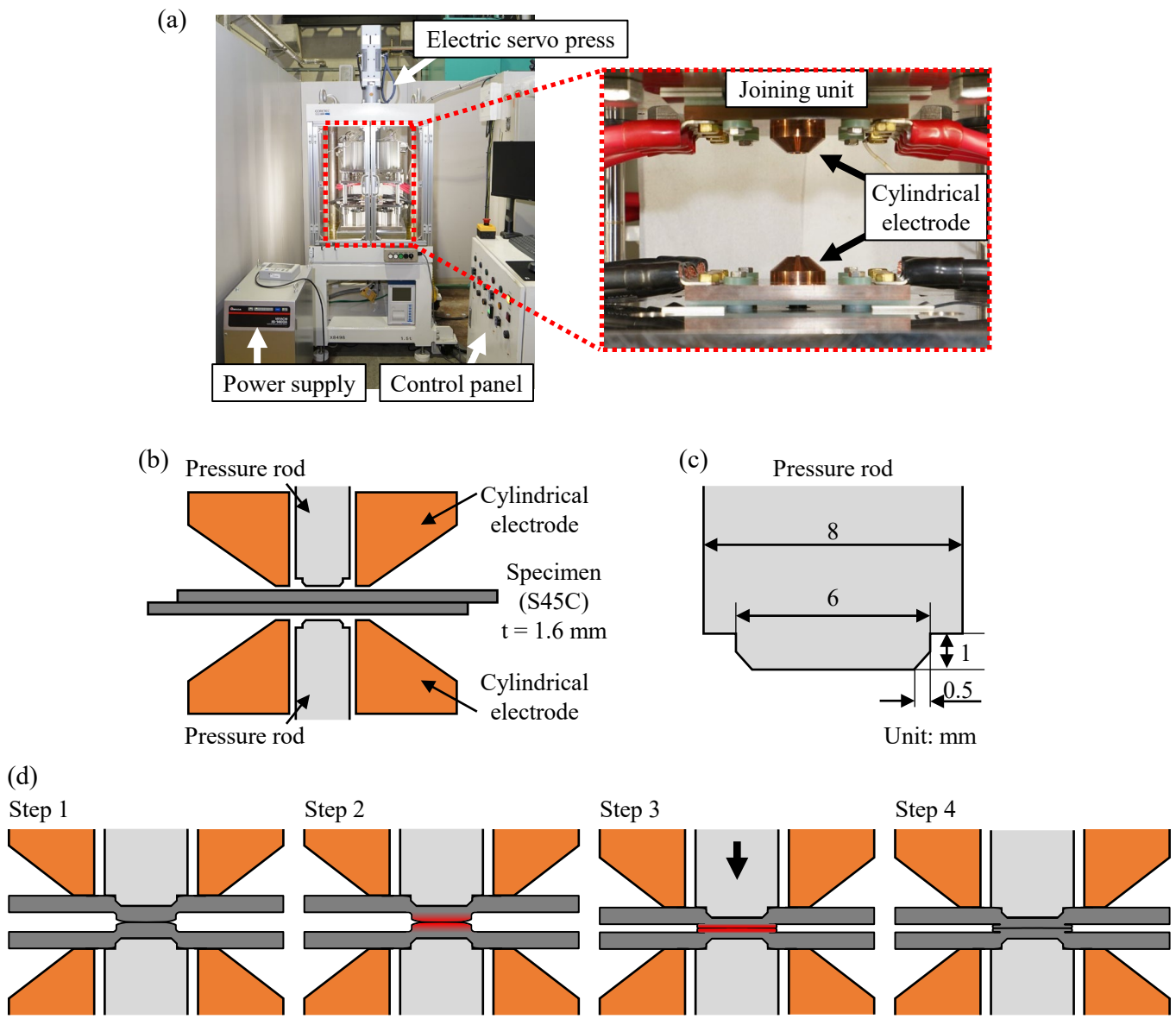

Figure 1. (a) Cold spot joining (CSJ) apparatus. (b) Cross-sectional view of the CSJ unit apparatus. (c) Tip of the central pressure rod. (d) Schematic illustration of the joining process for CSJ. Step 1: Pressure is applied with the central pressure rod and the copper electrode. Step 2: Current is applied and the temperature rises at the interface. Step 3: The material temperature rises, and the pressure applied by the pressure rod deforms the bonding material. Step 4: When the desired pressing amount is reached, energising and pressurising are stopped and the bonding is completed.

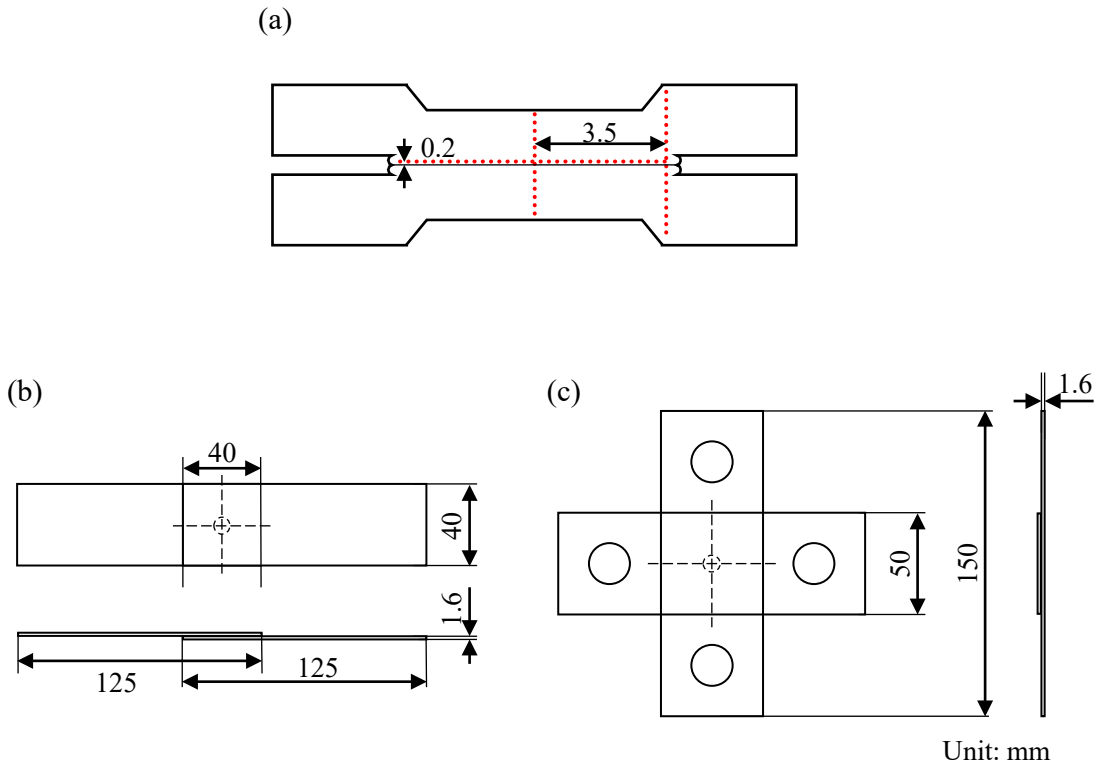

Figure 2. Schematic illustration of specimen preparation for (a) Vickers hardness measurements, (b) tensile shear test, and (c) cross-tension test.

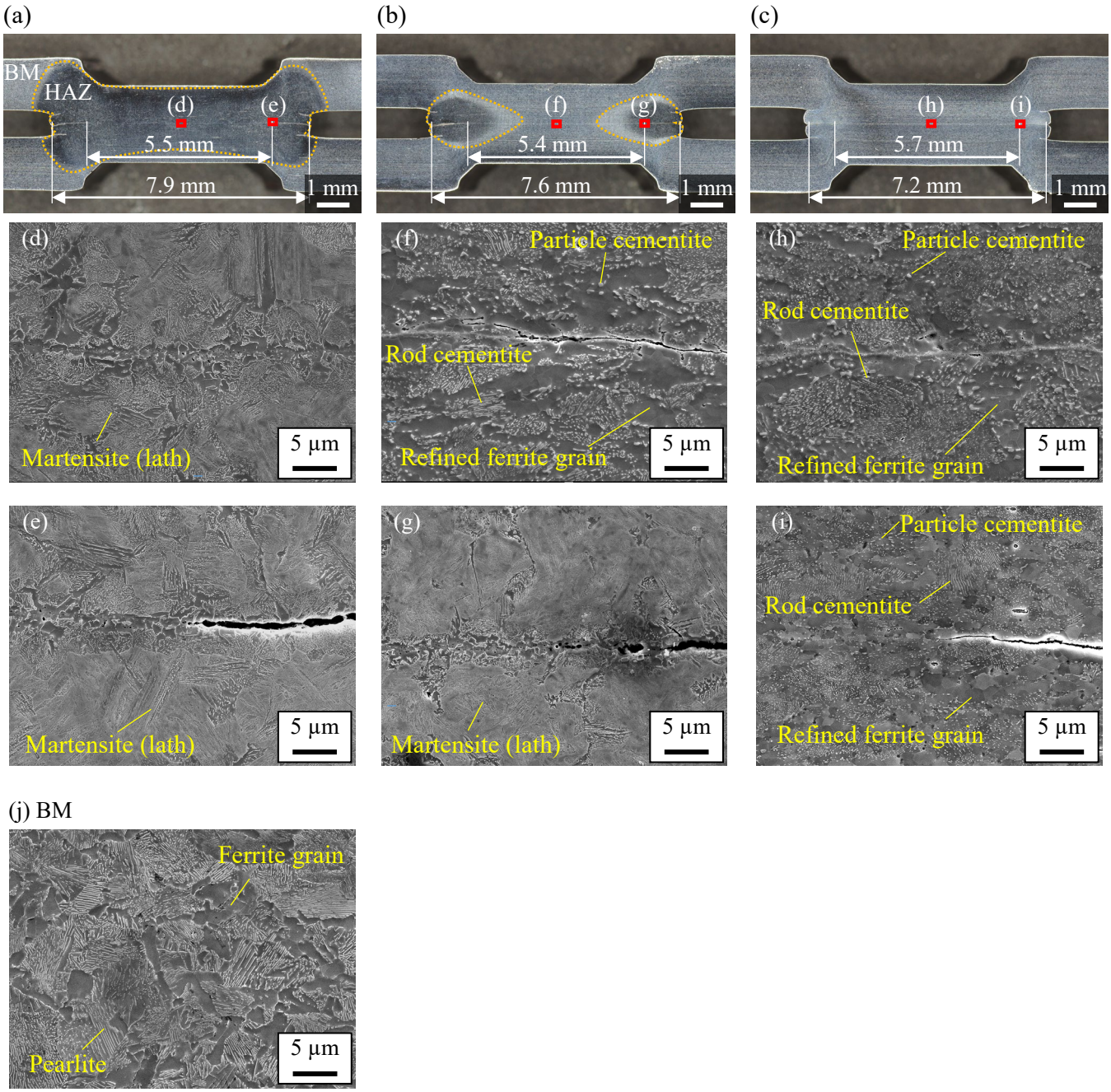

(j) BM

(k)

Applied pressure (MPa)	Pushing amount (mm)	Joining interface diameter (mm)	Junction region diameter (mm)
200	1.14	7.9	5.5
300	1.05	7.6	5.4
400	0.94	7.2	5.7

Figure 3. (a–c) Macrographs of cross-sections and scanning electron micrographs of the (d, f, h) joining interface centre and (e, g, i) periphery of the joints fabricated at applied pressures of 200, 300, and 400 MPa, respectively, with a constant 2500 A current. (j) Scanning electron microscopy image of the microstructure of S45C base material. (k) Pushing amount, joining interface diameter, and joining region diameter after joining at the applied pressures of 200, 300, and 400 MPa with a constant current of 2500 A.

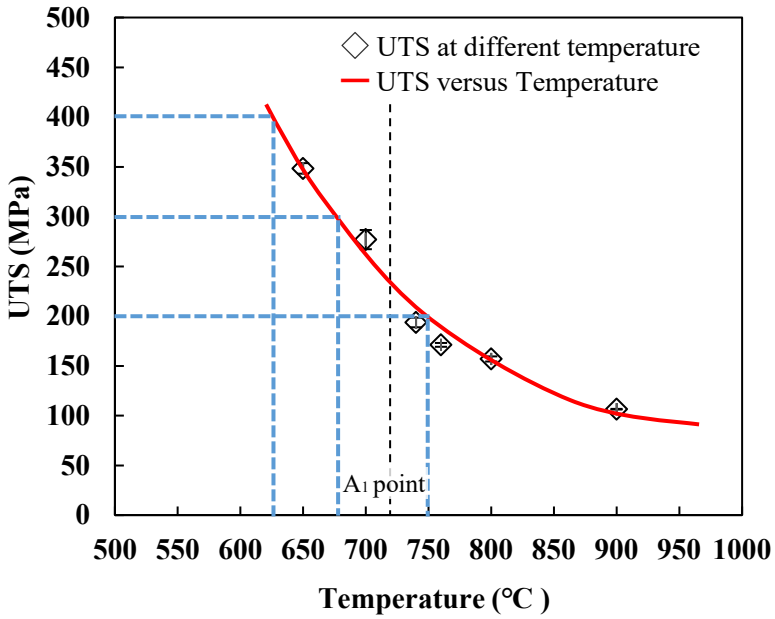

Figure 4. Temperature dependence of ultimate tensile strength (UTS) of S45C [17].

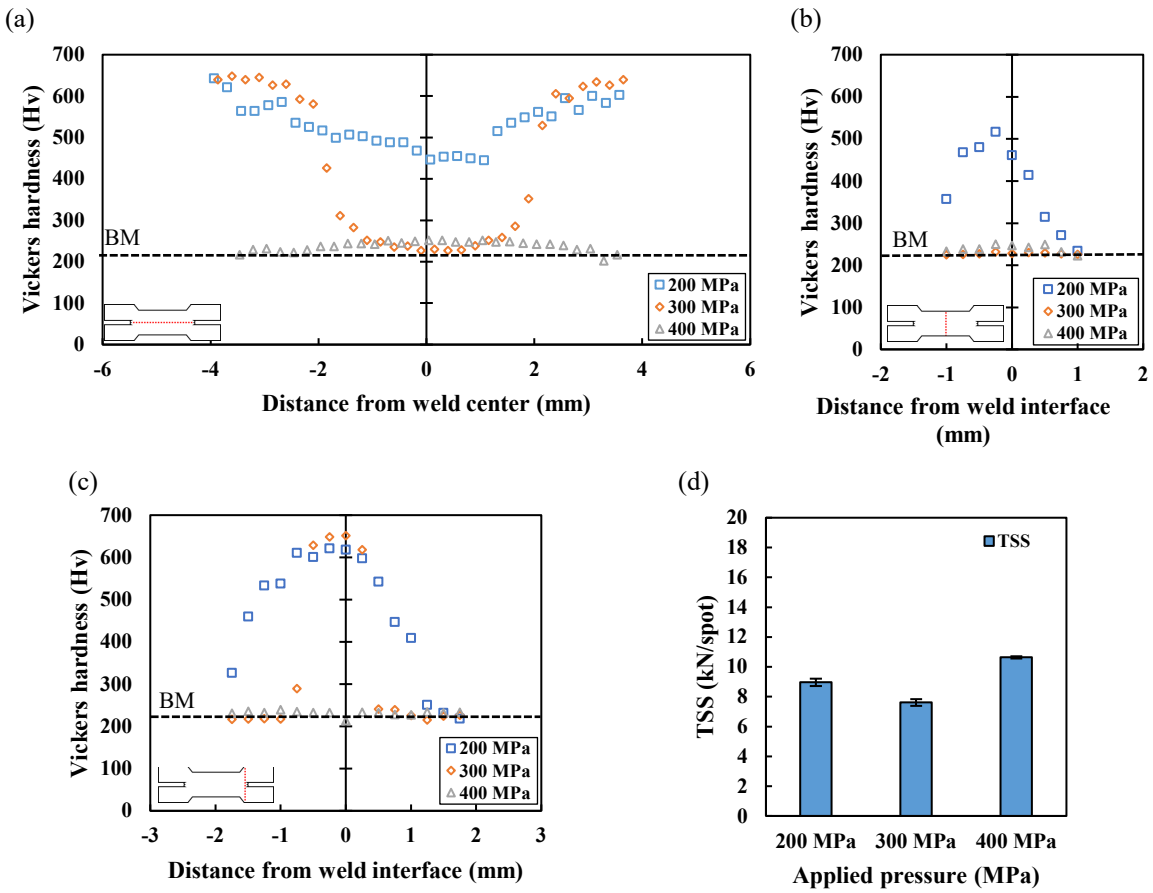

Figure 5. Hardness distributions along the (a) joining interface, (b) longitudinal axis at the centre, and (c) longitudinal axis at 3.5 mm from the centre on cross-sections of the joints fabricated at applied pressures of 200, 300, and 400 MPa with a constant 2500 A current. (d) Tensile shear strength of the joints fabricated at applied pressures of 200, 300, and 400 MPa with a constant 2500 A current.

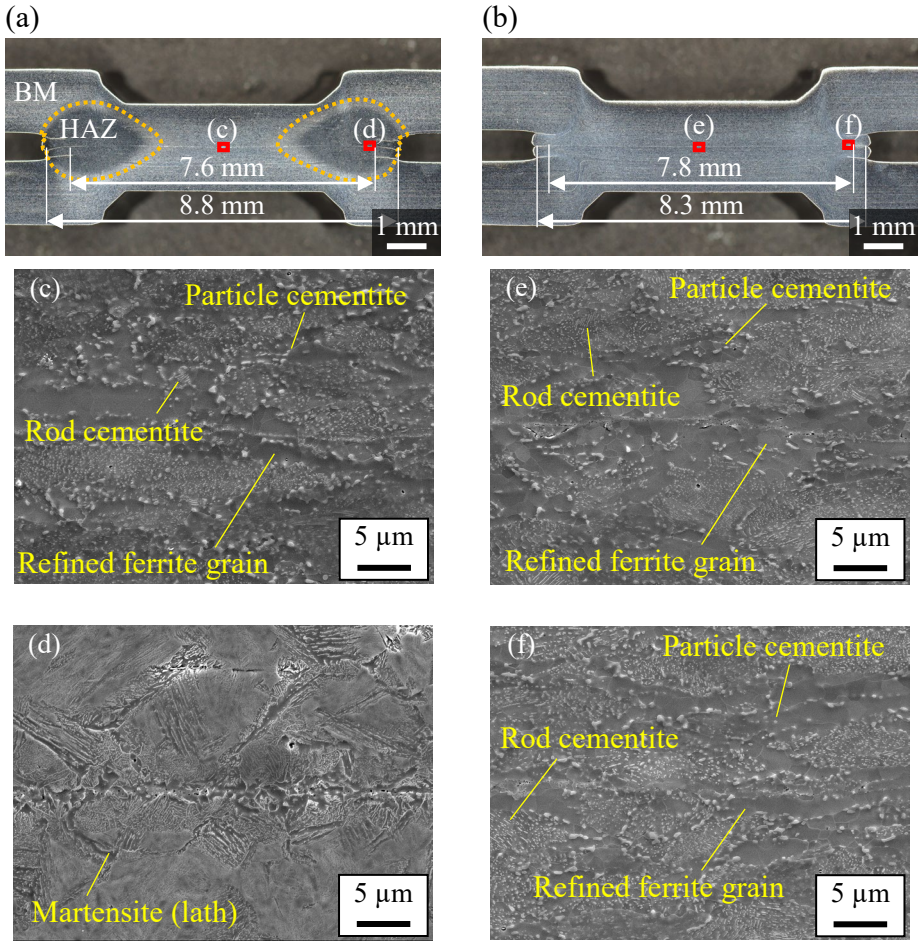

Figure 6. (a, b) Macrographs of cross-sections and (c–f) scanning electron micrographs of the joining interface centre and periphery of the joints fabricated at applied pressures of 300 and 400 MPa with a constant 1500 W power.

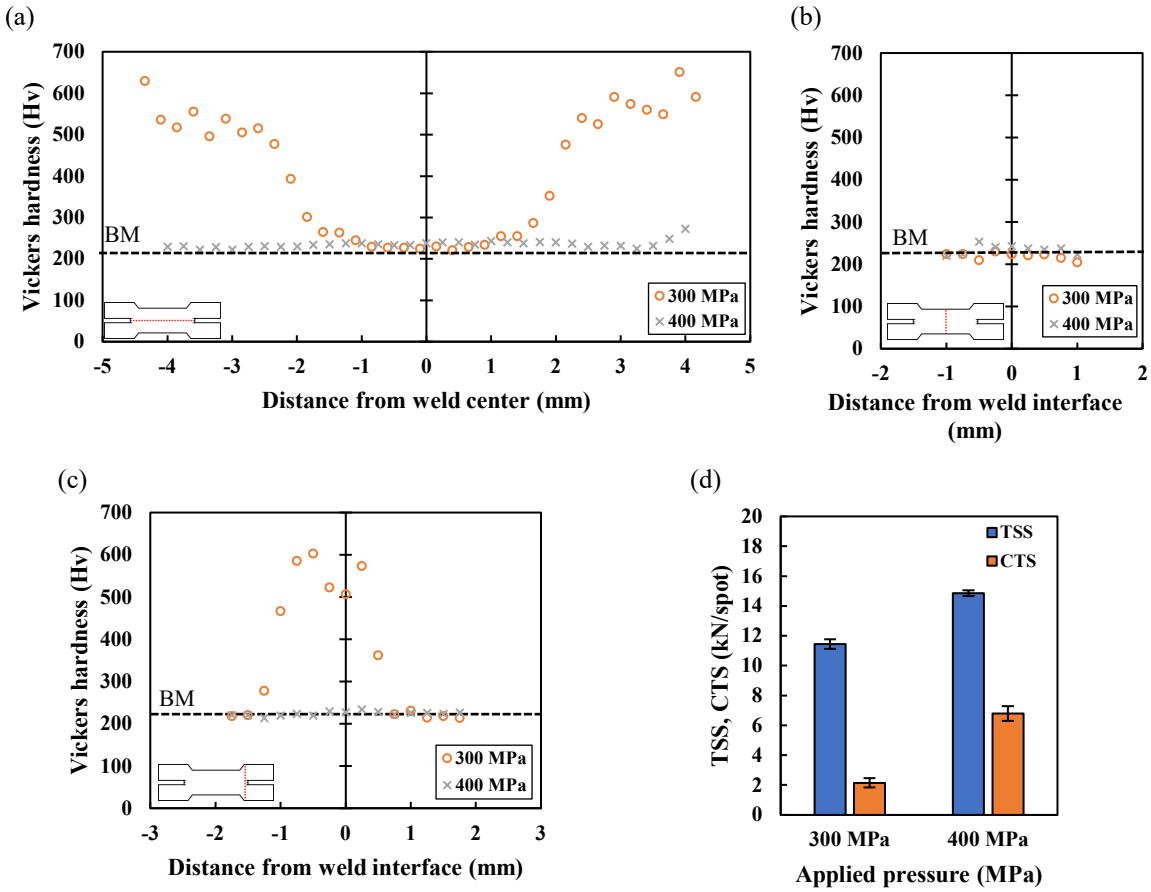

Figure 7. Hardness distributions along the (a) joining interface, (b) longitudinal axis at the centre, and (c) longitudinal axis at 3.5 mm from the centre on longitudinal cross-sections of the joints fabricated at different applied pressure of 300 and 400 MPa with constant 1500 W power. (d) Tensile shear strength (TSS) and cross-tension strength (CTS) of joints fabricated at different applied pressure of 300 and 400 MPa with constant 1500 W power.

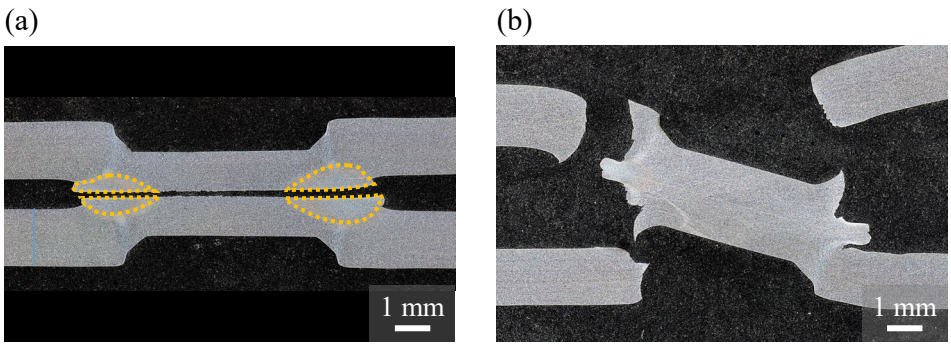

Figure 8. Macrographs of cross-sections after the cross-tension test of the joints fabricated at different applied pressure of (a) 300 and (b) 400 MPa with constant 1500 W power. The yellow dotted line indicates areas of martensite.